Rotational Diffusion and Order Parameters of a Liquid Crystalline Polymer Studied by ESR: Molecular Weight Dependence

Dajiang Xu, David E. Budil,[†] Christopher K. Ober,[‡] and Jack H. Freed*

Baker Laboratory of Chemistry, Cornell University, Ithaca, New York 14853-1301

Received: February 16, 1996; In Final Form: May 20, 1996[⊗]

The microscopic rotational dynamics of a main chain liquid crystalline (LC) poly(ether) in its nematic phase is studied in detail by nonlinear least squares analysis of ESR spectra in the slow motional regime. This complements results reported in an accompanying paper, which focuses on macroscopic translational diffusion using the DID-ESR (dynamic imaging of diffusion by ESR) technique. Far infrared 250 GHz ESR spectroscopy is used to determine the magnetic **g** and **A** tensors of the 3-carboxy-PROXYL spin label attached to the LC polymer. ESR spectra of the labeled polymers of varying molecular weights are analyzed to yield the rotational diffusion coefficients and orientational order parameters. Different cases of the degree of macroscopic alignment are observed in these samples and accounted for in the simulations. For molecular weights lower than 11 000 (for both tracers and matrices), the rotational diffusion coefficient $\bar{R}$ is found to correlate with the molecular weight of the polymer matrix and to be independent of the molecular weight of tracer, suggesting the importance of free volume for end-chain motion. Macroscopically aligned samples, corresponding to lower molecular weight LC polymers, show an inverse correlation of $\bar{R}$ with order parameter, consistent with observations previously reported for nonpolymeric LCs, which were associated with free volume effects.

1. Introduction

In the accompanying paper,[1] we have described translational diffusion measurements on a main chain semirigid liquid crystalline (LC) poly(ether) utilizing the technique of dynamic imaging of diffusion ESR (DID-ESR). We focused on the development of the DID-ESR technique for the macroscopic diffusion measurement of polydisperse polymers and its first application to LC polymeric materials. A model polymer was end labeled with a nitroxide free radical and served as a tracer, which diffused into the matrix of the same unlabeled polymer but of different molecular weight. The diffusive behavior of these samples is highly anisotropic, in addition to its dependence on the molecular weights of matrix and tracer species.[1] Such diffusional anisotropy indicates that the conformational properties of this class of materials play an important role in its macroscopic dynamics.

An advantage of DID-ESR over other techniques of diffusion measurement is the simultaneous availability of the standard ESR spectra on the same sample. Simulations by nonlinear least squares (NLLS) fitting of these ESR spectra can be utilized to yield microscopic motional and structural information. In this paper we study the rotational dynamics and orientational ordering in the same main chain semirigid LC poly(ether) samples that we studied by DID-ESR.

The methods used for ESR spectral line-shape analyses are described in detail in several papers.[2−4] This analysis involves four principal coordinate systems, the first two are rigidly fixed with respect to the molecular framework and are therefore referred to as molecular or body-fixed frames, whereas the latter two are space-fixed frames. They are (1) the principal molecular axis system (x''', y''', z''') of the magnetic tensors **A** and **g** of the spin label (by convention, x''' is defined as parallel to the N−O bond of the free radical and z''' is defined as parallel to the axis of N−O π orbital); (2) the molecular axis system (x', y', z') (which constitutes the principal axes of the rotational diffusion tensor); (3) the ordering axis system (x'', y'', z'') determined by the macroscopic nematic director $\bar{d}$ (a unit vector), which defines the preferred direction of molecular alignment in the sample; and (4) the laboratory axis system (x, y, z) with the z-axis along the static magnetic field. The tilt between the (x''', y''', z''') and the (x', y', z') molecular axis systems is represented by the Euler angles α, β, and γ. As a good approximation, (x', y', z') can be considered as an axially symmetric coordinate frame, in which the z'-axis coincides with the molecular long axis. The potential function $V(\Omega)$ determining the molecular ordering with respect to the nematic director $\bar{d}$ of a local domain can be expanded in a series of generalized spherical harmonics (also referred to as Wigner rotation matrices):

$$-\frac{V(\Omega)}{kT} = \sum_{L,M,K} \epsilon^L_{MK} D^L_{MK}(\Omega) = \epsilon_{20} D^2_{00} + \epsilon_{22}[D^2_{02}(\Omega) + D^2_{0-2}(\Omega)] + \epsilon_{40} D^4_{00} + \ldots \quad (1)$$

where Ω represents the Euler angles specifying the transformation between the molecular frame rotational diffusion axes (x', y', z') and the lab frame director axes (x'', y'', z''), k is Boltzmann's constant, T is the temperature, and (ϵ^L_{MK}), ϵ_{20}, ϵ_{22}, and ϵ_{40} are dimensionless potential coefficients of the respective Wigner rotation matrix elements $D^L_{MK}(\Omega)$. Also ψ represents the Euler angles referred to as the director tilt angle, i.e. the angles between the ordering axis z'' (the nematic director $\bar{d}$) and the magnetic field B_0 (z-axis). The relative orientations of these four coordinate systems are illustrated in Figure 1 along with a schematic structure of the end-labeled liquid crystalline polyether.

The microscopic properties determined by ESR in the present work include the rotational diffusion constants $R_{||}$ and $R_\perp$, for molecular motion about the directions parallel and perpendicular

[†] Present address: Dept. of Chemistry, Northeastern University, Boston, MA 02115.

[‡] Dept. of Materials Science and Engineering, Cornell University, Ithaca, NY 14853-1501.

[⊗] Abstract published in *Advance ACS Abstracts,* September 15, 1996.

S0022-3654(96)00514-X CCC: $12.00

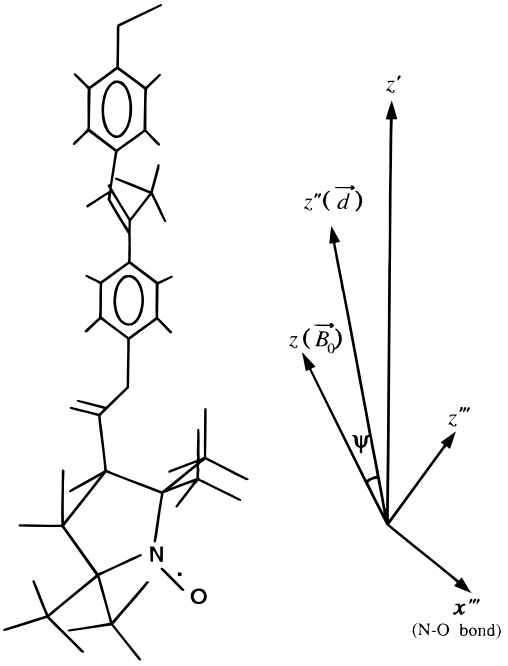

Figure 1. (a) Schematic structure of liquid crystalline random co-poly(ether) DHMS-7,9 end labeled with 3-carboxy-PROXYL. (b) The four coordinate systems used in the ESR spectral analysis including the laboratory axis z (defined as the direction of the static magnetic field B_0); the principal ordering axis z'' (determined by the nematic director $\vec{d}$); the principal molecular rotational diffusion axis z' (coincident with the backbone of the polymer molecule); the magnetic axis x''' (defined as parallel to the N−O bond); and z''' (defined as parallel to the axis of the N−O π orbital).

to $\hat{z}'$ (a unit vector along the z'-axis), respectively, and the orientational order parameter S. The purpose of NLLS fitting of theoretical simulations to the ESR spectra is to find the optimum values for $R_{||}$, $R_\perp$, ϵ_{20}, ϵ_{22}, and ϵ_{40}. After the potential coefficients are determined, the orientational order parameter S is obtained from its definition as the ensemble average of $D^2_{00}(\Omega)$:

$$S \equiv \langle D^2_{00}(\Omega)\rangle = \langle (3\cos^2\theta - 1)/2\rangle = \int d\Omega D^2_{00}(\Omega) \exp\left[-\frac{V(\Omega)}{kT}\right] \Big/ \int d\Omega \exp\left[-\frac{V(\Omega)}{kT}\right] \quad (2)$$

where $\theta = \cos^{-1}(z'\cdot\vec{d})$ is the angle between the molecular long axis and the direction of liquid crystalline ordering. Thus, S ranges in value from 1 (for perfect ordering with $z'||\vec{d}$) to -0.5 with perfect alignment of $z'\perp\vec{d}$. S will be used to refer either to the macroscopic ordering of the LC polymer or to the local ordering within microscopic domains of an unaligned sample. In the macroscopically aligned samples studied, the nematic director $\vec{d}$ of each domain coincides with the direction of the spectrometer field B_0. Samples that are not macroscopically aligned are analyzed using a model of microscopic order macroscopic disorder (MOMD)[5] in which the microscopic directors have a uniform distribution of orientations in the lab frame, as illustrated in Figure 2.

The first step of the spectral analysis is to determine the magnetic **g** and **A** tensors of the spin label. One usually starts with a rigid limit spectrum in which the motion is "frozen" and the lineshape is solely determined by the magnetic **g** and **A** tensors. Far infrared 250 GHz ESR (FIR-ESR) is a very effective way to separate the x''', y''', z''' components of the **g** tensor, and it also can provide better resolution for the **A** tensor than X-band ESR.[6] It will be assumed that the **g** and **A** tensor values are independent of temperature and the molecular weights of the samples. Thus, once the magnetic tensors of the spin label are determined, their values are fixed throughout all the simulations of the ESR spectra obtained at temperatures where the rotational motions tend to average out the spectral effects of the **g** and **A** tensors. We calculate an ESR spectrum based on the input parameters, which include the parallel and perpendicular rotational diffusion coefficients $R_{||}$ and $R_\perp$, the potential coefficients, the diffusion tilt β, and the inhomogeneous Gaussian line-width broadening Δ. A modified Marquardt−Levenberg algorithm[7−9] was used to iterate the simulations until a minimum least squares fitting to experiment is reached, and this provides the optimum values for the fitted parameters, as well as estimates of error.[9,10]

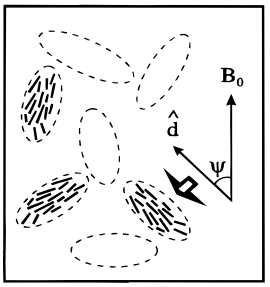

Figure 2. Schematic of the MOMD (microscopic order macroscopic disorder) model in the nematic phase of a liquid crystalline polymer. The "director tilt" angle ψ between the magnetic field B_0 and the director $\vec{d}$ of the local domain is randomly distributed.

In the analysis of these ESR spectra, three different cases are distinguished according to the degree of macroscopic alignment of the samples, as discussed earlier.[1] In this paper, we examine relationships between the microscopic and macroscopic properties and the effect of the matrix and tracer on the rotational behavior in this nematic LC poly(ether) DHMS-7,9, and we compare the results with those from ordinary (nonpolymeric) liquid crystals and with the macroscopic translational diffusion coefficients.

2. Experiment

2.1. Materials. Samples for the X-band ESR measurements are the same ones that were used for measuring the translational diffusion coefficients as reported in the accompanying paper.[1,11] The synthesis and physical properties of the nine model polymer samples, which are semi-rigid main chain LC poly(ether)s DHMS-7,9 end labeled with 3-carboxy-PROXYL, can be found in ref 1 (cf. Table 2 in ref 1).

The sample used in the 250 GHz FIR-ESR experiment was a labeled DHMS-7,9 ($M_w = 3300$, $M_n = 2700$, $T_m = 87$ °C, $T_{ni} = 125$ °C) mixed with an unlabeled polymer ($P_w = 6500$, $P_n = 4900$, $T_m = 105$ °C, $T_{xn} = 113$ °C, $T_{ni} = 137$ °C) to reduce the spin concentration, where M_w (M_n) are the weight (number) average molecular weights of the tracer, P_w (P_n) are the weight (number) average molecular weights of the matrix, T_m is the melting transition temperature, T_{xn} is the transition temperature from an intermediate phase (exhibited in some materials) to the nematic phase,[1] and T_m is the transition temperature from the nematic to the isotropic phase. An unlabeled polymer of lower molecular weight ($P_w = 3000$, $P_n = 2400$, $T_m = 80$ °C, $T_{ni} =$

126 °C) was used to dilute the same labeled DHMS-7,9 (M_w = 3300), in order to obtain the hyperfine splitting A_0 by X-band ESR measurements on the isotropic phase (153 °C). This sample will be referred to as sample 10.

2.2. Measurement and Data Analysis. All X-band ESR spectra were measured on the same spectrometer that was used for DID-ESR experiments with the same temperature control apparatus.[1] The spectra of nine DID-ESR samples were taken at the beginning and the end of each DID-ESR experiment at 120 ± 1 °C in the absence of a magnetic field gradient, with a modulation amplitude less than 0.5 G and a data acquisition time a little longer than 2 min. The time constant was 0.25 *s*, and the other settings (microwave power, sweep width, modulation frequency) were the same as those used for the DID-ESR experiments. The same conditions were used to measure A_0 from sample 10 except that the temperature was 153 °C, corresponding to the isotropic phase.

The high-field rigid limit spectrum was obtained on a 250 GHz FIR-ESR spectrometer described elsewhere.[6] This experiment was carried out at −155 ± 2 °C with a time constant of 1 *s*, a modulation amplitude of about 1 G at 89 kHz frequency, and a sweep field of about 482 G. The spectrum was digitized to 1281 data points. The actual magnetic field values were calibrated by a FIR-ESR spectrum of a standard perdeuterated Tempone (PDT) in toluene-d_8 sample at room temperature, whose splitting had been accurately measured previously.[12]

Spectra were analyzed to obtain the ordering and rotational dynamics utilizing ESR spectral simulation methods based on the stochastic Liouville equation.[2−5] The simulations were fit to the experimental data utilizing a modified Levenberg−Marquardt NLLS minimization algorithm to obtain the optimum ESR parameters.[9,10]

All spectral simulations were performed on IBM RS6000 RISC computers at the Cornell Theory Center and the Cornell Materials Science Center.

3. Results and Discussion

3.1. The Magnetic Parameters of the Spin Label. The 250 GHz ESR rigid limit spectrum at −155 °C of labeled DHMS-7,9 is shown in Figure 3. It enables one to directly read off the **g** tensor components from the spectrum as indicated by the upper axis in the figure. Note that the three components g_i (i = x‴, y‴, z‴) of the **g** tensor in its principal frame are given by

$$h\nu = g_i\beta_e B_i \qquad (3)$$

where h is Planck's constant, ν is the frequency of the resonant radiation (ν = 249.90 GHz), β_e is the Bohr magneton, and B_i is the resonant magnetic field value of each component. The $g_{z'''}$ region at the high-field side of the spectrum also yields the three-line hyperfine splitting (hfs) corresponding to $A_{z'''}$. The $g_{x'''}$ region at the low-field side of the spectrum shows two peaks that are much larger than the $A_{x'''}$ hfs for a nitroxide. We have found that $g_{x'''}$ is very sensitive to the "local polarity" and/or to conformational effects.[13] It is also sensitive to local site inhomogeneities.[13b] One reason for this is that $\Delta g_{x'''} \equiv (g_{x'''} - g_e)$ is the largest, so it shows the most site variation. It is suggested that the two peaks could be due to two different configurations or two different types of microscopic regions in the polymer. $A_{y'''}$ could be determined accurately from the field positions of the extrema associated with the central spectral component corresponding to $g_{y'''}$ in association with the NLLS simulations noted below. The resolution of the spectrum shown in Figure 3 is insufficient to obtain $A_{x'''}$, partly due to the dual peaks and partly due to the increased line width in the x'''-region most likely due to a distribution in $g_{x'''}$ values arising from site inhomogeneities within the sample (so-called *g*-strain), which is much more significant at 250 GHz than at 9 GHz ESR. To obtain $A_{x'''}$, a fast motional ESR spectrum at the X-band was taken from sample 10 at 153 °C to determine its isotropic hfs A_0. Then $A_{x'''}$ was obtained from

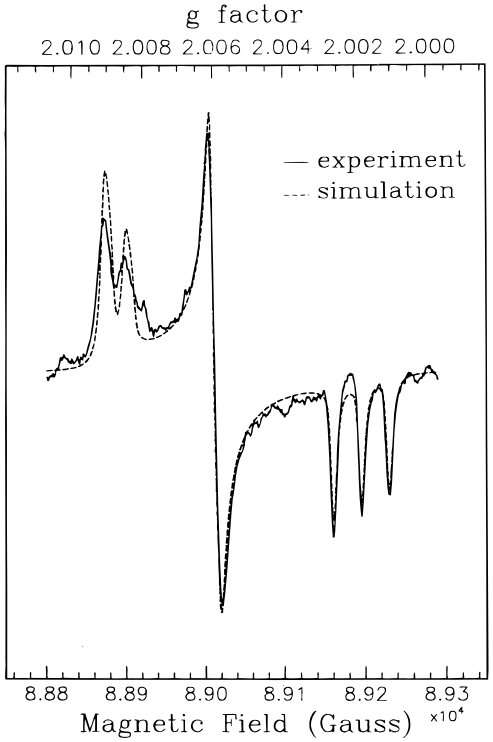

Figure 3. Rigid limit 250 GHz ESR spectrum of LC poly(ether) DHMS-7,9 at −155 °C. The magnetic parameters were measured directly from the spectrum: $g_{y'''}$ = 2.0060; $g_{z'''}$ = 2.0018; $A_{z'''}$ = 34.37 G; with the two $g_{x'''}$ of 2.0090 (65%) and 2.0084 (35%). The dashed line is the simulated spectrum as described in the text.

TABLE 1: Magnetic Parameters of 3-Carboxy-PROXYL Attached to the End of DHMS-7,9[a]

	x'''	y'''	z'''
g	2.0088[b]	2.0060	2.0018
A (G)	5.2	4.3	34.4

[a] Estimated error in *g* tensor components is ±1 × 10^{-4}. For the *A* tensor components, it is ±0.3G. [b] This is the average of the two observed values of 2.0090 (65% relative population) and 2.0084 (35% relative population).

$$A_{x'''} + A_{y'''} + A_{z'''} = 3A_0 \qquad (4)$$

These magnetic parameters were refined by NLLS simulations of the rigid limit spectrum,[6] as is also shown in Figure 3. The relative populations of the two components corresponding to the different $g_{x'''}$ values were also determined by a least squares analysis.[9] The magnetic parameters and relative populations are given in Table 1. For the X-band motional studies the parameters listed in Table 1 were utilized. Since there was no indication in the 9 GHz X-band spectra of two sites, we utilized an average $g_{x'''}$. (Note that X-band spectra are about 30 times less sensitive to **g** values than is 250 GHz ESR due to the much reduced magnetic fields.)

3.2. Rotational Diffusion and Ordering Parameter. In the accompanying paper[1] we described the different degrees of macroscopic alignment obtained for the DID-ESR samples with the 3 kG magnetic fields utilized in X-band ESR experiments.

Accordingly, we needed to consider three different cases to simulate these spectra in order to determine the rotational diffusion coefficients and the orientational order parameters. These cases are (cf. Table 2) (1) macroscopically aligned (samples *AD*, *BD*, *AE*, and *BE*); (2) MOMD (samples *CD* and *CE*); and (3) a mixture of aligned and MOMD (samples *AF*, *BF*, and *CF*).

Macroscopically Aligned DHMS-7,9. This case is the most sensitive to the fitting parameters. Therefore, we selected this group to determine the transformation between the magnetic frame axes (x''', y''', z''') and the rotational diffusion axes (x', y', z'). As stated earlier, this transformation could be fully described by the three Euler angles α, β, and γ. However, the efficiency of the spectral calculation is significantly improved when α and γ are zero. Therefore an approximation was made by which the (x', y', z') axes were permuted and a "diffusion tilt angle" β was allowed to vary in the fitting procedure. The minimal set of parameters includes the parallel and perpendicular rotational diffusion coefficients, $R_{||}$ and $R_\perp$, the primary potential term ϵ_{20} corresponding to cylindrically symmetric ordering, the diffusion tilt angle β, and the inhomogeneous Gaussian line-width broadening, Δ, with the magnetic parameters given in Table 1. The spectral simulation provided minimum deviation from the experimental data for the permutation of the (x', y', z') axes in which $y''' \parallel z'$ (so-called *y*-ordering), and we found the fitted value of β was $10° \pm 5°$. In the *y*-ordering case, the z'-axis is perpendicular to the z'''-axis and β represents the angle between x' and z'''. After the best approximations for these angles were made, it was fixed (i.e. *y*-ordering and $\beta = 10°$) for the non-linear least squares fits reported in this paper. Also, the director tilt angle, ψ, is zero for the macroscopically aligned samples.

The splittings of the ESR spectra are very sensitive to the ordering, given the same values for the other parameters. On the other hand, the line widths of the ESR spectra were found to depend mainly on the perpendicular rotational diffusion coefficient, $R_\perp$, and to be less sensitive to the parallel rotational diffusion coefficient, $R_{||}$, as judged by the significantly larger uncertainties estimated for this parameter by the NLLS program.[9] The anisotropy ratio of rotational diffusion N ($N = R_{||}/R_\perp$)) was found to be about 2−4 in most cases. Thus, to reduce the uncertainty in the fits resulting from correlations between $R_\perp$ and $R_{||}$ and to conveniently simplify the analysis, $N = 3$ was used for all spectra and the geometric averaged rotational diffusion $\bar{R}$ ($\bar{R} = [R_\perp{}^2 R_{||}]^{1/3}$), was varied in the final fits to experiment. Similarly the Gaussian line width, Δ, was also approximately constant for the different samples, but exhibited substantial correlations with other fitting parameters, so it was convenient to fix it at the average value of 0.8 G.

Thus, in all the final NLLS fits to experiment, including the next two groups, the following parameters were fixed: $N = 3$; $\beta = 10°$; $\Delta = 0.8$ G. After $\bar{R}$ and ϵ_{20} were fit, the higher order terms in the potential, ϵ_{22} and ϵ_{40}, were introduced into the simulation mainly for fine adjustment of the relative peak heights of the $M_I = \pm 1$ lines. Each such procedure was restarted several times with different seed values in order to check the convergence to a unique minimum, as well as to avoid entrapment of the NLLS search algorithm in a false local minimum. The orientational order parameter S was then calculated according to eq 2. The experimental and simulated ESR spectra are plotted in Figure 4. The values of $\bar{R}$ and S that were obtained are listed in Table 2. We also list the values of the translational diffusion coefficient, $\langle D_i \rangle$, that was obtained by DID-ESR as described in ref 1.

We observe that $\bar{R}$ appears to depend significantly on matrix molecular weight; that is, it is 1×10^8 s^{-1} for matrix P_w of 4600 and 2×10^8 s^{-1} for matrix P_w of 7800, but it is rather independent of the tracer molecular weight (of 4000 or 8600). One might expect that this is a free volume effect such that the larger molecular weight matrix provides more void space for the tracer. Meanwhile, a larger tracer is likely to have less rotational mobility. Actually the free volume in ordinary LC systems has been found to be dependent on the order parameter, S,[15−19] yielding the following expression for a rigid spin probe:

$$\bar{R} = \bar{R}^0 \exp[-AS^2/RT] \qquad (5)$$

corresponding to an activation energy, which is proportional to S^2. (Here R is the universal gas constant.) While we do not have sufficient results to test the applicability of this equation

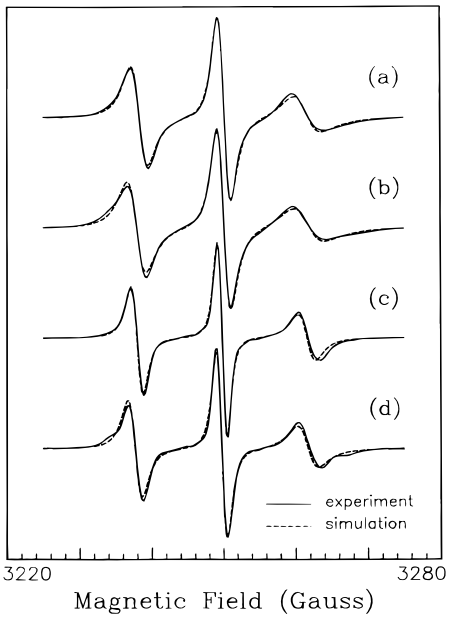

Figure 4. Experimental and simulated ESR spectra for aligned samples. Parts a, b, c, and d are from DID-ESR samples *AD*, *BD*, *AE*, and *BE*, respectively. Their molecular weights and fitting parameters are listed in Table 2.

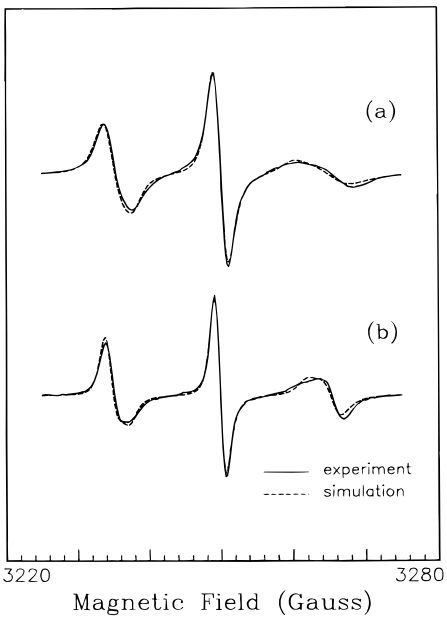

Figure 5. Experimental and simulated ESR spectra for MOMD samples. Parts a and b are from DID-ESR samples *CD*, and *CE*, respectively. Their molecular weights and fitting parameters are listed in Table 2.

TABLE 2: Diffusion Coefficients and Order Parameters of DHMS-7,9

sample[a]	matrix (P_w)	tracer (M_w)	$\langle D_i \rangle^b$ ($\times 10^9$) (cm^2/s)	S^c	$\bar{R}^c$ (10^8 s^{-1})	fitting model
AD	4600	4000	110	0.416	1.28	aligned
BD	4600	8600	15	0.355	1.15	aligned
CD	4600	13400		0.112	1.14	MOMD
AE	7800	4000	16	0.318	1.99	aligned
BE	7800	8600	6.7	0.258	2.09	aligned[d]
CE	7800	13400	3.1	0.188	2.4	MOMD
AF	30700	4000	7.6	0.255	1.7	35% aligned, 65% MOMD
BF	30700	8600	1.7	0.258	1.6	39% aligned, 61% MOMD
CF	30700	13400		0.247	1.9	23% aligned, 77% MOMD

[a] The samples are the same as those used in the DID-ESR measurements, reported in ref 1 (cf. Table 2 of ref 1 and ref 11). The estimated error in P_w and M_w is about 5%. [b] The diffusion coefficients listed here are from ref 1. The estimated error is ±10%. [c] The error in $\bar{R}$ and S was calculated assuming a normal distribution of residuals and then scaling by the reduced χ^2 of the fits as described in ref 9. The average percent errors to the NLLS parameters are $\epsilon_{\bar{R}}R = 3.6$ and $\epsilon_S = 0.8$ for the first five entries and $\epsilon_{\bar{R}}R = 10$ and $\epsilon_S = 2.6$ for the last four entries. [d] The fitting of this spectrum required a small MOMD component (relative intensity = 10%) that was assumed to have the same fitting parameters as the aligned portion.

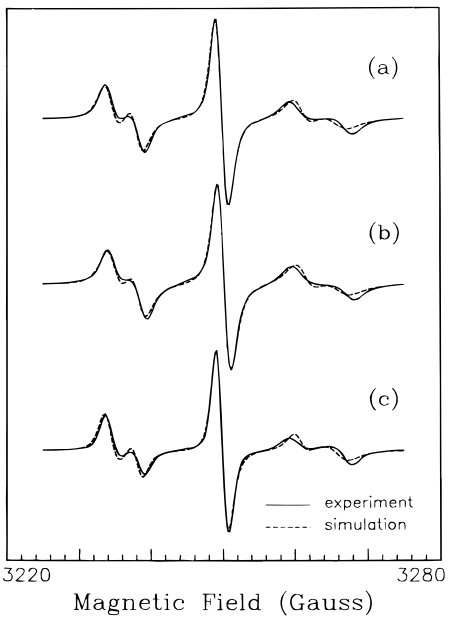

Figure 6. Experimental and simulated ESR spectra for samples with aligned and MOMD components. Parts a, b, and c are from DID-ESR samples *AF*, *BF*, and *CF*, respectively. Their molecular weights and fitting parameters are listed in Table 2.

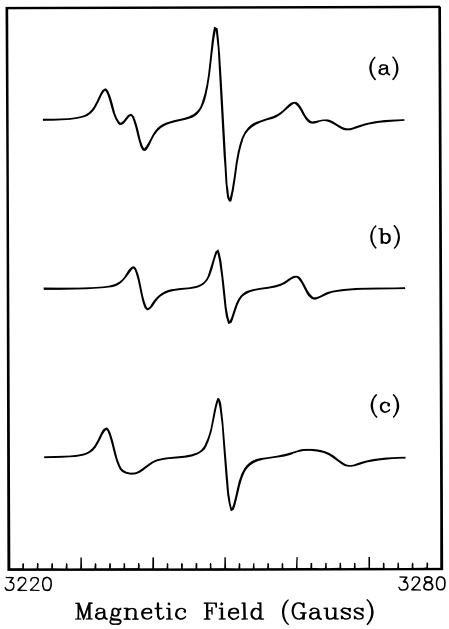

Figure 7. (a) Simulated ESR spectrum in Figure 6a. (b) Macroscopically aligned component in part a. (c) MOMD component in part a.

for the polyethers, we do indeed see from Table 2 that S is larger in the lower molecular weight matrix corresponding to the smaller values of $\bar{R}$.

Microscopic Order Macroscopic Disordered (MOMD) DHMS-7,9. For MOMD samples, the nematic directors of all local domains have a uniform distribution of orientations, while there exists liquid crystalline ordering within each microscopic domain. The order parameter S refers to local ordering in the MOMD case. The simulation procedure is similar to the one used for macroscopically aligned samples, except that the calculated spectrum is a superposition of spectra corresponding to different ψ values.[5] We find that usually it is sufficient to average 10 spectra with ψ ranging from 0° to 90°. The rotational diffusion and order parameters of the two MOMD samples are listed in Table 2. Both the experimental and simulated ESR spectra are plotted in Figure 5.

The order parameters obtained from both samples are quite different. As such, the influence of microscopic ordering on the diffusional processes is unclear at this stage. However, we do note that values of $\bar{R}$ of about 1×10^8 and 2×10^8 s^{-1} are again obtained with matrices of molecular weight of 4600 and 7800, respectively, just as we observed in aligned samples even though a tracer of higher molecular weight, 13 400, was used. We suspect that a free volume model may still be appropriate, but eq 5 developed for ordinary LCs would no longer be valid for larger tracers, especially since it was obtained for more rigid types of molecules, whereas in the present experiments the spin label is attached to the flexible end-chain of the polymer. The reorientational motion of the end-chain should depend more on the void space available to it in the matrix rather than on the length of the rest of the polymer chain to which it is attached.

DHMS-7,9 Samples with Aligned and MOMD Components. The limited resolution of the ESR spectra resulting from the overlap of the two components did not permit us to fit each component independently with its ordering and rotational diffusion parameters. Therefore, the simulations for this case were carried out by assuming that both the macroscopically aligned and MOMD components had the same values for rotational diffusion and order parameters. With this constraint imposed, the relative population of each component was fitted along with $\bar{R}$ and the potential coefficients. The results are listed in Table 2 with the spectra plotted in Figure 6. The fits in this case, while reasonable, are a little less satisfactory than in the previous two cases, possibly due to the fitting constraints imposed by the reduced resolution. The simulated spectra from each component are shown separately in Figure 7 for the case of Figure 6a. Those for Figure 6b,c are very similar, so they are not shown here.

Note that the two-component ESR pattern was observed only from samples with the largest molecular weight of the matrix (30 700). The relative populations of the aligned component and the order parameter are about the same in these samples. There does not appear to be much dependence of $\bar{R}$ on tracer (but this could reflect the less satisfactory fits in this case).

4. Summary

In summary, we find that for the lower molecular weight matrices ($P_w = 4587$ and 7800) the average rotational diffusion coefficient $\bar{R}$ increases with increasing P_w but is independent of tracer molecular weight in the range of $M_w = 4000$ to 13422. There is some indication of an inverse correlation between $\bar{R}$ and S in the lower molecular weight polymer samples, which would be consistent with observations on nonpolymeric LCs. The $\bar{R}$ is a microscopic property reflecting the reorientational motion of the end-chain, so it need not necessarily correlate with macroscopic measurement of $\langle D_i \rangle$, as we observe. Since the best fits to experiment are obtained from macroscopically aligned spectra, it is recommended that in future studies efforts are made to achieve good alignment even for samples of higher molecular weight by aligning in strong (e.g. 9 T) magnetic fields, prior to performing the X-band ESR experiments. In an accompanying paper[20] we describe how the modern technique of two-dimensional Fourier-transform ESR enables us to examine in greater detail the molecular dynamics of these samples, and we also describe temperature dependent studies.

Acknowledgment. We would like to gratefully thank Dr. E. Hall for her numerous helpful discussions and the supply of the DHMS-7,9 samples and Dr. R. H. Crepeau for his help in preparation of the manuscript. This work was supported by the MRL Program of the National Science Foundation under Award No. DMR-9121654 and by NSF Grant No. DMR-9210638. The Cornell Theory Center and the Cornell Materials Science Center are also acknowledged.

References and Notes

(1) Xu, D.; Hall, E.; Ober, C. K.; Moscicki, J. K.; Freed, J. H. *J. Phys. Chem.* **1996**, *100*, 15856.

(2) Schneider, D. J.; Freed, J. H. In *Biological Magnetic Resonance*; Berliner, L. J.,Reuben, J., Plenum: New York, 1989; Vol. 8, p 1.

(3) Meirovitch, E.; Freed, J. H. *J. Phys. Chem.* **1984**, *88* (21), 4995.

(4) Freed, J. H. in *Spin Labeling: Theory and Applications*; Berliner, L. J., Ed.; Academic Press: New York, 1976; p 53.

(5) Meirovitch, E.; Nayeem, A.; Freed, J. H. *J. Phys. Chem.* **1984**, *88* (16), 3454.

(6) (a) Budil, D. E.; Earle, K. A.; Freed, J. H. *J. Phys. Chem.* **1993**, *97* (7), 1294; b) Earle, K. A.; Budil, D. E.; Freed, J. H. *J. Phys. Chem.* **1993** *97* (50), 13289.

(7) Dennis, J. E., Jr.; Schnabel, R. B. *Numerical Methods for Unconstrained Optimization and Nonlinear Equations*; Prentice-Hall: Englewood Cliffs, NJ, 1983.

(8) More, J. J.; Garbow, B. S.; Hilstron, K. E. *User's Guide for MINPACK-1*; National Technical Information Service: Springfield, VA, 1980.

(9) Budil, D. E.; Lee, S.; Saxena, S.; Freed, J. H. *J. Magn. Res.* **1996**, *A120*, 155.

(10) (a)Crepeau, R. H.; Rananavare, S. B.; Freed, J. H. Automated Least-Squares Fitting of Slow Motional ESR Spectra. *Abstracts of 11th International EPR Symposium*, Rocky Mountain Conference, Denver, CO, 1987. (b) Shin, Y.-K.; Freed, J. H. *Biophys. J.* **1989**, *55*, 537.

(11) Two more samples (in addition to the seven DID-ESR samples) used in the current study were made from tracer *C* and matrices *D* and *F* (cf. Tables 1 and 2 of ref 1). They are referred to as samples *CD* and *CF*, respectively.

(12) Hwang, J. S.; Mason, R. P.; Hwang, L-P.; Freed, J. H. *J. Phys. Chem.* **1975**, *79* (5), 489.

(13) (a) Earle, K. A.; Moscicki, J. K.; Ge, M.; Budil, D. E.; Freed, J. H. *Biophys. J.* **1994**, *66*, 1213. (b) Budil, D. E.; Earle, K. A.; Lynch, W. B.; Freed, J. H. *Advanced EPR: Applications to Biology and Biochemistry*; Hoff, A. J., Ed; Elsevier: Amsterdam, 1989; Chapter 8.

(14) Press, W. H.; Flannery, B. P.; Teukolsky, S. A.; Vetterling, W. T. *Numerical Recipes: The Art of Scientific Computing*; Cambridge Univ. Press: Cambridge, 1986.

(15) Shin, Y.-K.; Moscicki, J. K.; Freed, J. H. *Biophys. J.* **1990**, *57*, 445.

(16) Shin, Y.-K.; Budil, D. E.; Freed, J. H. *Biophys. J.* **1993**, *65*, 1283.

(17) Moscicki, J. K.; Shin, Y.-K.; Freed, J. H. *J. Chem. Phys.* **1993**, *99* (1), 634.

(18) Freed, J. H.; Nayeem, A.; Rananavare, S. B. in *The Molecular Dynamics of Liquid Crystals*; Luckhurst, G. R., Veracini, C. A., Eds.; Kluwer Academic Publishers: Netherlands, 1994; Chapter 13.

(19) Freed, J. H. *Annu. Rev. Biophys. Biomol. Struct.* **1994**, *23*, 1.

(20) Xu, D.; Crepeau, R. H.; Ober, C. K.; Freed, J. H. *J. Phys. Chem.* **1996**, *100*, 15873.

JP960514D